

Anomalous Jet Tagging via Sequence Modeling

Alan Kahn[†], Julia Gonski[†], Inês Ochoa[‡], Daniel Williams[†], Gustaaf Brooijmans[†]

[†]Nevis Laboratories, Columbia University in the City of New York, USA

[‡]Laboratory of Instrumentation and Experimental Particle Physics, Lisbon, Portugal

Abstract

This paper presents a novel method of searching for boosted hadronically decaying objects by treating them as anomalous elements of a contaminated dataset. A *Variational Recurrent Neural Network* (VRNN) is used to model jets as sequences of constituent four-vectors. Coupled with a carefully considered pre-processing, the VRNN gives each jet an *Anomaly Score* that distinguishes between the substructure of signal and background jets. The model is trained in an entirely unsupervised setting and without high level variables, making the score more robust against mass and p_T correlations when compared to traditional substructure-based methods. Performance is evaluated on the jet level, as well as in an analysis context by searching for a heavy resonance with a final state of two boosted jets. The Anomaly Score shows consistent performance along a wide range of signal contamination amounts, for both two- and three-pronged jet substructure hypotheses. Analysis results demonstrate that the use of Anomaly Score as a classifier enhances signal sensitivity while retaining a smoothly falling background jet mass distribution. The model's discriminatory performance resulting from an unsupervised training scenario opens up the possibility to train directly on data without a pre-defined signal hypothesis.

1 Introduction

The frontier of high energy physics has many open questions, such as the nature of dark matter or the origin of matter-antimatter asymmetry, which are being explored by the ATLAS and CMS Experiments at the Large Hadron Collider (LHC). Since the discovery of the Higgs boson in 2012 [1, 2], no signals of new beyond the Standard Model (BSM) physics have been found. Sophisticated analysis tools utilizing novel machine learning models are key to detecting rare signals that may be missed by traditional methods.

Machine learning is being consistently integrated into new physics searches at the LHC. While many applications focus on classifying known signatures, such as top quarks or Higgs bosons, there are a number of emerging techniques aimed at the discovery of new particles. Many of these techniques use classifier models to search for particular model hypotheses, by training and evaluating a model using Monte Carlo simulation of the BSM signal. While these models show promising performance, they are subject to inaccuracies between simulated samples and data, which occur most severely in the non-perturbative regime of QCD processes.

One way to circumvent these inaccuracies is to develop a model that trains directly on data, without requiring the need for simulated inputs. Distinguishing new physics from Standard Model background at the LHC without a signal hypothesis is a novel and promising effort [3]. This paper demonstrates a way to identify BSM signals that present as anomalous substructure in jets using unsupervised, data-driven anomaly detection.

Anomaly detection refers to a process in which anomalous elements are identified within a dataset that is mostly homogenous, but contaminated with outliers. In a machine learning context, this can be done with a model that learns an underlying distribution of data points, as characterized by high-level features of the data. Such a model can then identify out-of-distribution data solely on how poorly they are represented by the learned underlying distribution. Several candidate architectures have been developed for this purpose. The examination of their features is instructive in choosing an architecture for the specific task presented here.

1.1 Autoencoders

A popular candidate architecture for anomaly detection is the *autoencoder* (AE) [4], which has been previously studied in a particle physics context. Autoencoders are an example of a generative model in which a network is trained to reconstruct a given input. Figure 1 shows an example of a standard AE architecture.

A key feature of autoencoders is a latent layer in the center of the architecture which is often of a lower dimensionality than the input, directly restricting the network’s ability to perfectly reconstruct its input. In such a case, the network achieves its training goal best when it can represent high-level features of the input as vectors, or *codes*, in its latent space. The accuracy with which each code represents the input can be verified by decoding it, and comparing its result with the original input. In this way, the AE is considered to act as two neural networks being trained in parallel: an *encoder* network f which acts as the map from data to the latent space, $\mathbf{z} = f(\mathbf{x})$, and a *decoder* network g which then attempts to reconstruct the original input from its encoded representation, $\mathbf{y} = g(\mathbf{z})$. The loss function of the AE can be any function of

the form $\mathcal{L}(\mathbf{x}, \mathbf{y} = g(f(\mathbf{x})))$, which is minimal when $\mathbf{y} = \mathbf{x}$. A common choice is the *Mean Squared Error* (MSE) between the input and output of the autoencoder:

$$\mathcal{L} = \|\mathbf{y} - \mathbf{x}\|^2 \quad (1)$$

In the context of anomaly detection, elements which represent a small portion of a dataset will contribute less during the training process. As a result, they will be less represented by the learned codes when compared to elements belonging to the majority class of data. One can therefore expect the reconstruction of anomalous elements to be worse, placing them in the tails of the loss function's distribution after training. This principle has been explored in anomalous jet tagging, for instance by representing the jets as images [5], or as lists of constituents [6].

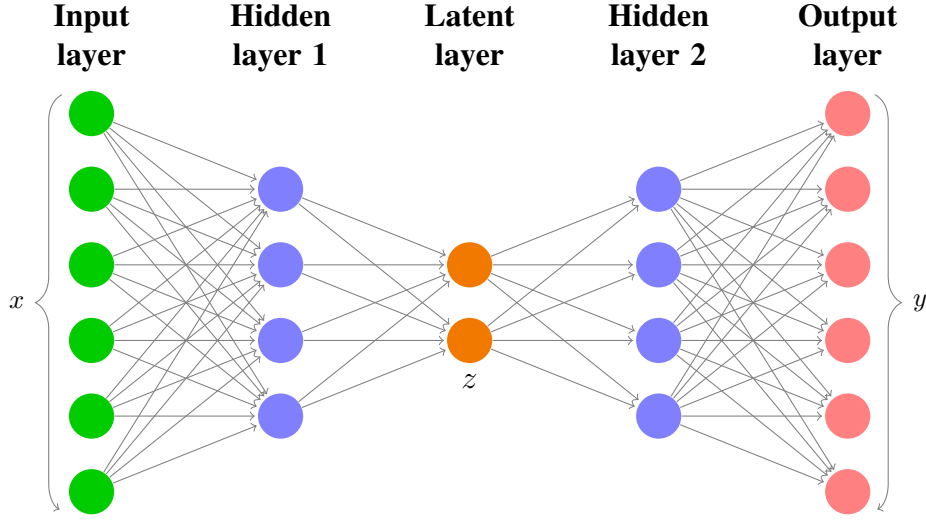


Figure 1: A standard autoencoder.

1.2 Variational Autoencoders

Variational Autoencoders (VAEs) are built on the idea of standard AEs, with the extension that they are designed to perform Bayesian inference. This assumes that observed data \mathbf{x} is generated by some hidden random variable \mathbf{z} whose posterior distribution $p(\mathbf{z}|\mathbf{x})$ is intractable. The goal of a VAE is to learn an approximate posterior distribution, $q(\mathbf{z}|\mathbf{x})$, through training.

The architecture of a VAE is very close to that of a standard autoencoder. The main difference is a latent space that can accommodate an encoder, which maps data to a distribution in the latent space rather than a single vector. A common choice for the form of the latent space is a multivariate Gaussian of diagonal covariance. In this case, the encoder can map a given input to two independent layers, each with the same dimensionality as the latent space. One of these layers represents the means of the encoded Gaussian distribution while the other represents the respective standard deviations. Decoding then requires sampling from this resulting distribution. This can be easily performed in the case of a Gaussian approximate posterior by use of the *reparametrization trick*. Instead of sampling the distribution directly, a particular value of z can be represented in the following way:

$$z = \mu + \sigma\epsilon \quad (2)$$

where ϵ is sampled from a unit isotropic normal distribution $\epsilon \sim \mathcal{N}(0, 1)$ [7].

The VAE performs Bayesian inference by determining the marginal likelihood, which is the result of an often intractable calculation:

$$p(x) = \int p(z)p(x|z)dz \quad (3)$$

By using Bayes' Theorem, and inserting the approximate posterior distribution $q(z|x)$, the log likelihood can be expressed in terms of two Kullback-Leibler (KL)-Divergences, one from a prior distribution $p(z)$ to the approximate posterior $q(z|x)$, and the other from the true posterior distribution $p(z|x)$ to the same approximate posterior $q(z|x)$. The remaining term is the log likelihood of data, and can be interpreted as the reconstruction accuracy of generating x from the underlying variable z .

$$\begin{aligned} \log(p(x)) &= \mathbb{E}_Z[\log p(x)] \\ &= \mathbb{E}_Z \left[\log \frac{p(x|z)p(z)}{p(z|x)} \right] \\ &= \mathbb{E}_Z \left[\log \frac{p(x|z)p(z)}{p(z|x)} \frac{q(z|x)}{q(z|x)} \right] \\ &= \mathbb{E}_Z[\log p(x|z)] - \mathbb{E}_Z \left[\log \frac{q(z|x)}{p(z)} \right] + \mathbb{E}_Z \left[\log \frac{q(z|x)}{p(z|x)} \right] \\ &= \underbrace{\mathbb{E}_Z[\log p(x|z)]}_{\text{Reconstruction Error}} - \underbrace{\int q(z|x) \log \frac{q(z|x)}{p(z)} dz}_{D_{KL}(q(z|x)||p(z))} + \underbrace{\int q(z|x) \log \frac{q(z|x)}{p(z|x)} dz}_{D_{KL}(q(z|x)||p(z|x))} \end{aligned} \quad (4)$$

While the true posterior distribution is still intractable, the KL-Divergence is by definition non-negative. The first two terms of this result can therefore be described as a lower bound on the evidence. When this lower bound is maximized, the remaining intractable KL-Divergence approaches zero, corresponding to a situation in which the reconstruction error is zero, and the approximate posterior is equivalent to the true posterior. Therefore, the negative of this lower bound is chosen as the loss function of the VAE, and is minimized through training. The reconstruction error term is chosen to be the mean-squared-error loss as used in the ordinary AE. The total loss function therefore takes the following form:

$$\mathcal{L} = |\mathbf{y} - \mathbf{x}|^2 + D_{KL}(q(z|x)||p(z)) \quad (5)$$

For the prior, it is common to choose a unit isotropic Gaussian centered at the origin, as the KL-Divergence between a Gaussian approximate posterior and a Gaussian prior takes on a closed form solution [8].

Variational Autoencoders provide a number of improvements over standard Autoencoders, both as a generative model [7] and as an anomaly detection tool [9]. The inclusion of a KL-Divergence term in the loss function motivates the architecture to more appropriately model unique classes of data. It also acts as another discriminatory metric, as anomalous elements are expected to have both a large reconstruction error and a large KL-Divergence when compared to nominal elements.

While VAEs have shown promise in the task of jet-level anomaly detection, they have a number

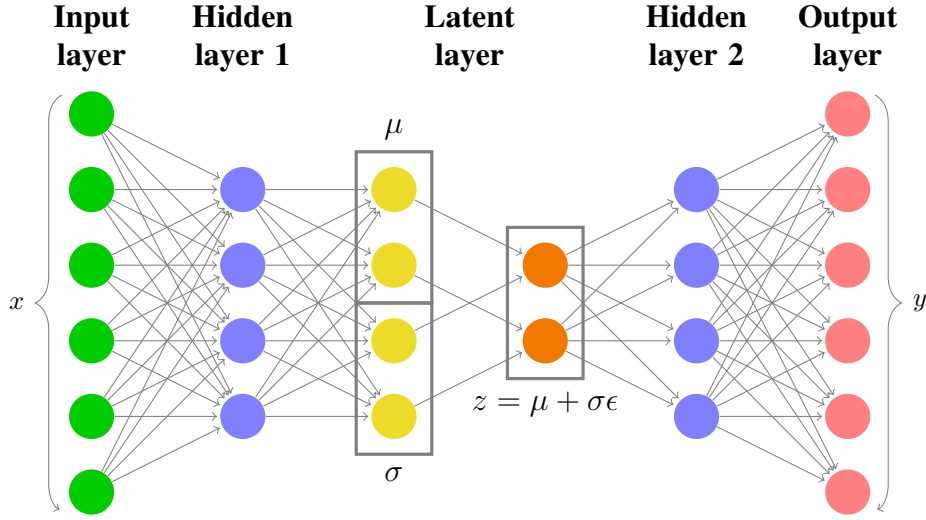


Figure 2: A Variational Autoencoder with a Gaussian latent space parametrization.

of drawbacks. Most notably, VAEs are a fixed-length architecture, and cannot accommodate a variable number of inputs. When modeling jets via their constituent four-vectors, it becomes necessary to only process at most N constituents, and *zero-pad* the input layer when processing a jet with a number of constituents less than N . In classifier models, this is common and benign, as the loss function depends only on the output of the network and the ground truth that it is trying to reproduce. However, in a VAE, the input layer's neuron values are a part of its loss function (due to the MSE loss between the input and output layers). Therefore, the zero padded elements directly correlate with the value of the loss function. This introduces a direct correlation between the VAE loss and the number of constituents in the input jet which can be difficult to remove.

A recurrent architecture naturally circumvents this drawback since it is designed to accommodate inputs of varying length. In a *Recurrent Neural Network* (RNN), data is input as a sequence of features. Each feature has the same fixed dimensionality, yet the sequence itself can vary in length. The RNN is comprised of a chain of small fixed architectures, or *cells*, which expect as inputs the fixed-length feature at each element, or *time-step*, in the sequence. While processing the sequence, the RNN updates a *hidden state* at each time-step, which is carried over and accessed by the cell during the following time-step. The hidden state stores a long-term representation of information within the sequence, and is the key feature allowing RNNs to process sequential data of varying length. The RNN cell then acts as an encoder-decoder architecture which inputs the current time-step's feature and hidden state, and outputs an updated hidden state, along with an output feature if desired. In the interest of performing anomaly detection using a recurrent architecture, the model in this study has been chosen to be one which combines the recurrent property of RNNs with the VAE's ability to perform variational inference.

2 Variational Recurrent Neural Network

The Variational Recurrent Neural Network (VRNN) used in this study is a sequence modeling architecture which replaces the encoder-decoder step of a traditional RNN with a VAE. An illustration of one VRNN cell can be seen in Figure 3. In this model, the VAE's input at each

time-step is given as the vector $x(t)$, which is then encoded and decoded into an output vector $y(t)$ which can be compared to $x(t)$ via the reconstruction loss. The ϕ_x and ϕ_z layers represent *feature-extracting layers*, which are interpreted as learned representations of the features of the input $x(t)$ and the encoded latent space distribution $z(t)$, respectively. After each time-step, the hidden state is updated via a recurrence relation, in which the current hidden state $h(t-1)$ and the current set of extracted features ϕ_x and ϕ_z produce an updated hidden state $h(t)$ via the following equation [10]:

$$h(t) = f(\phi_x, \phi_z, h(t-1)) \quad (6)$$

Performing this particular step is the primary function of traditional RNN architectures such as Long Short-Term Memory Networks (LSTMs) [11] and Gated Recurrent Units (GRUs) [12].

The VAE present in each cell of the VRNN notably differs from conventional VAEs in the following ways:

1. The encoder and decoder are conditioned on the current time-step's hidden state. This is represented by the concatenation operation between the hidden state $h(t-1)$ and the feature-extraction layers ϕ_x and ϕ_z .
2. The prior from which the KL-Divergence is computed is no longer a unit Gaussian at the origin, but rather a multivariate Gaussian whose means and variances in each dimension are determined from the current time-step's hidden state.

The inclusion of a learned, time-dependent prior distribution is an important component of the VRNN architecture. Without this feature, the decoder network would only be able to access information about the current time-step from the hidden state, and the loss function would motivate the posterior distributions for each time-step to be identical. As a result, this allows the VRNN the flexibility to model complex structured sequences with high variability, as is expected from a jet represented by a sequence of constituent four-vectors. In more detail, each time-step's latent space prior distribution parameters μ_t and σ_t are functions of the current time-step's hidden state:

$$z_t \sim \mathcal{N}(\mu_t, \sigma_t), \text{ where } \mu_t, \sigma_t = f^{prior}(h_{t-1}) \quad (7)$$

Similarly, the latent space approximate posterior is defined by parameters μ and σ which are functions of the input's extracted features ϕ_x and the hidden state h_{t-1}

$$z \sim \mathcal{N}(\mu, \sigma), \text{ where } \mu, \sigma = f^{post.}(\phi_x, h_{t-1}) \quad (8)$$

The generated output is then decoded from features extracted from the latent space distribution $\phi_z = f(z)$, while also being conditioned on the hidden state

$$y(t) = f^{dec}(\phi_z, h(t-1)) \quad (9)$$

A loss for each time-step $\mathcal{L}(t)$ can then be computed by incorporating both the reconstruction error between the input constituent $x(t)$ and generated output constituent $y(t)$, as well as the KL-Divergence between the approximate posterior z and the learned prior z_t . A constant λ is also included which weights the KL-Divergence term's contribution to the loss.

$$\mathcal{L}(t) = |y(t) - x(t)|^2 + \lambda D_{KL}(z || z_t) \quad (10)$$

An overall loss \mathcal{L} over the sequence is then computed by averaging the individual time-step losses over the length of the sequence N

$$\mathcal{L} = \frac{\mathcal{L}(t)}{N} \quad (11)$$

This loss function performs the same role as the VAE’s loss function, acting both as an appropriate means of optimizing the architecture as well as a discriminatory quantity between nominal and anomalous elements of the dataset.

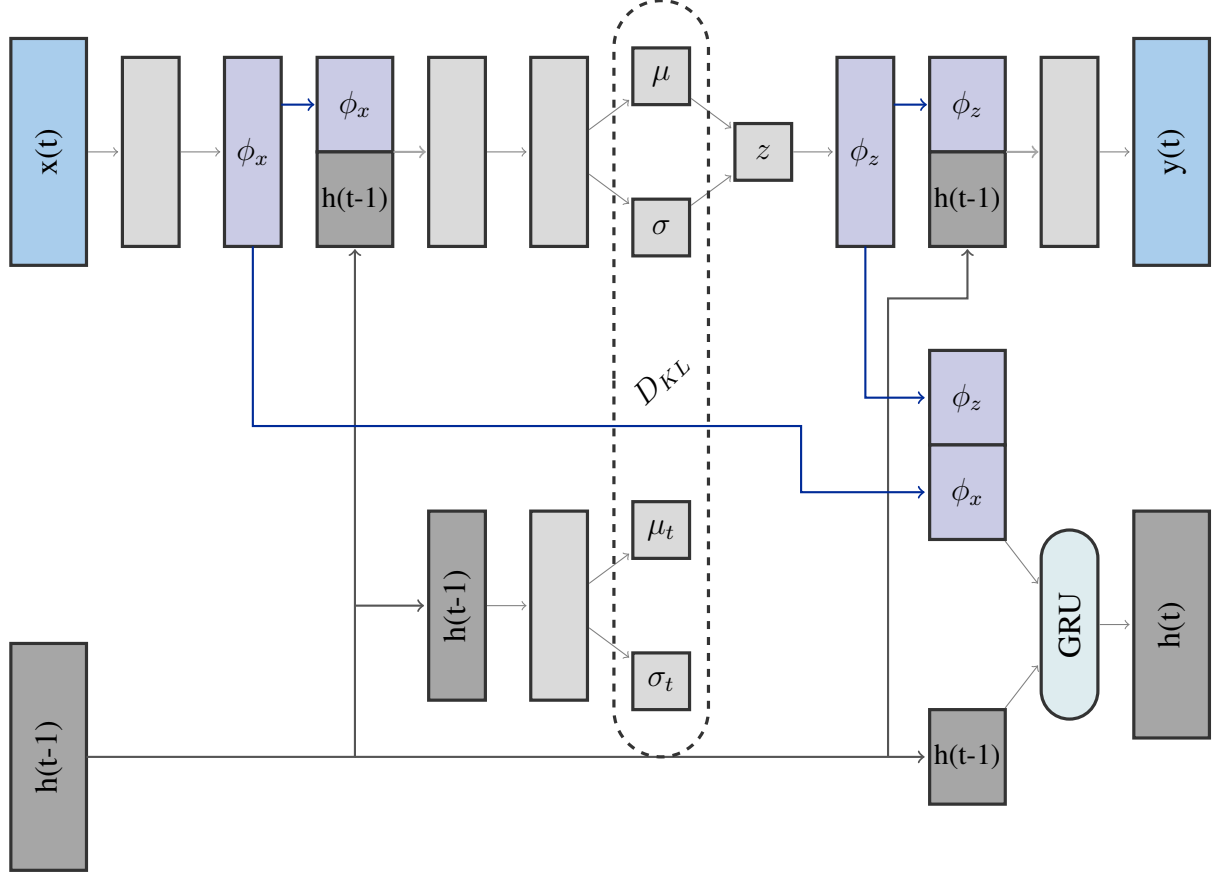


Figure 3: A Variational Recurrent Neural Network cell.

The details of the VRNN architecture used in this study are as follows: The number of neurons in each intermediate layer, including the hidden state and feature extracting layers, but not including the latent space and its μ and σ layers, is 16. The latent space is chosen to be two-dimensional. Since constituent four-vectors of jets are being modeled, the input $x(t)$ and output $y(t)$ layers are three dimensional, corresponding to the $p_T, \eta,$ and ϕ of each constituent. ReLU activations are used in each layer of the network, except for σ and σ_t , which have softmax activations, and z and $y(t)$, which have linear activations.

The constituents of an input jet are processed sequentially, one per each time-step. Each time-step contributes a loss based on the VAE loss function:

$$\mathcal{L}(t) = MSE + \lambda D_{KL} \quad (12)$$

where λ is a factor which weights the KL-Divergence contribution relative to the MSE reconstruction loss. Since harder constituents contribute more information toward the identification of jet substructure, λ is defined to be a function of constituent p_T fraction such that lower p_T constituents obtain a lower weight in the loss function. Furthermore, since a constituent's p_T

fraction depends directly on the number of constituents in the jet, the distribution of p_T fractions for each constituent in the jet is averaged over all respective constituents in the entire input dataset to avoid correlations with constituent multiplicity.

In this result, the loss is therefore computed for each constituent as:

$$\mathcal{L}(t) = MSE + 0.1\overline{p_T}(t)D_{KL} \quad (13)$$

where MSE is the mean-squared-error between $x(t)$ and $y(t)$, D_{KL} is the KL-Divergence from the current time-step's prior distribution and the encoded posterior, and $\overline{p_T}(t)$ is the p_T of the dataset-averaged constituent at time-step t . The final loss is computed by averaging the individual time-step losses over the entire jet:

$$\mathcal{L} = \frac{\sum \mathcal{L}(t)}{N} \quad (14)$$

The hyperparameters involved in this implementation, namely the dimensionality of intermediate layers, and the additional weight coefficient of 0.1 in the loss function were determined via a hyperparameter optimization scan.

After the network is trained, an *Anomaly Score* can be determined for each jet. The KL-Divergence term has been shown to provide better discrimination between anomalous and standard jets than either the reconstruction error or the loss term as a whole. Therefore, the Anomaly Score is defined in terms of the KL-Divergence of each constituent, averaged over the whole jet, and restricted to the range of (0, 1) via exponentiation.

$$\text{Anomaly Score} = 1 - e^{-\overline{D_{KL}}} \quad (15)$$

3 Data Samples and Pre-Processing

The performance of the model is investigated by studying its ability to discriminate signal from background in a contaminated dataset of background QCD dijet events with varying amounts of signal. The signal events are a process of the form of $Z' \rightarrow XY \rightarrow JJ$ where X and Y are two heavy resonances each decaying into a boosted jet J . Two types of signal events are generated. One type is comprised of events where the X and Y both decay to two quarks, resulting in boosted jets with two-pronged substructure. The other type differs in that the X and Y both decay to three quarks, resulting in boosted jets with three-pronged substructure. The masses of the particles in the signal hypothesis are 3.5 TeV, 500 GeV, and 100 GeV for Z' , X , and Y respectively. A total of 99457 signal events were generated for each substructure hypothesis, along with 995,453 background events. The events were generated using PYTHIA8 and the detector response was simulated using DELPHES 3.4.1 with no pile-up or multiple parton interactions included, and selected using a single large-radius ($R=1$) jet trigger with a p_T threshold of 1.2 TeV. The dataset was provided as part of the LHC Olympics challenge for the ML4Jets2020 Workshop [13].

The data is provided as a list of hadrons for each event. The hadrons were then clustered into jets using the anti- k_t jet-clustering algorithm with a radius parameter of 1.0 [14]. In this study, only the highest p_T (leading) and second-highest p_T (sub-leading) jets are included in each event. To test the model's performance with varying amounts of signal contamination, contaminated datasets were produced with 13 different signal event fractions, 10 of which were generated in the range of 0.01% to 10.0% along a logarithmic scale, with three higher signal event frac-

tions of 25%, 50%, and 75%. For contamination levels up to and including 10%, contaminated datasets were created using the same set of background events while only the amount of signal is varied to match the desired contamination. This corresponds to a total of 895113 background events to accommodate the highest contamination level of 10%. For the three higher contamination levels, contaminated datasets were created using the same 99457 signal events while the number of background events are limited to 298641, 99457, and 33152 for 25%, 50%, and 75% contamination respectively. Three datasets are generated at each level of contamination: a contaminated dataset containing both signal and background events, a background-only validation set, and a signal-only signal set. Independent datasets are generated for both two-prong and three-prong signal substructure hypotheses at each level of contamination.

Since the goal is to identify jets mainly due to their substructure, it is important that the model’s Anomaly Score does not correlate with other jet features, namely mass and p_T . A common practice to avoid such a correlation in neural network jet modeling architectures is the use of adversarial de-correlation networks [15]. Applying such adversarial architectures to a VRNN is a complex task which is outside of the scope of this study [16]. Instead, this is achieved through a carefully considered pre-processing procedure, which can be divided into two steps: one which directly removes mass and p_T information from the input jets, and another which orders constituents in a way that improves the VRNN’s discriminatory performance.

3.1 Boosting

The pre-processing method is developed to produce jets which are superficially identical, with the only differences appearing in the arrangement of their constituents due to varying substructure. This procedure is inspired by a study based on jet images, where a pre-processing method which boosts each jet to the same reference frame allows for a model trained on the pre-processed jets to be robust against variations in mass and p_T [17]. The process can be briefly summarized in three steps:

- Rescale each jet to the same mass,
- Boost each jet to the same energy,
- Rotate each jet to the same orientation in η, ϕ .

Algorithm 1 describes in detail the implementation of the rescaling, boosting, and rotating processes, or simply *boosting* for short.

Algorithm 1: Jet Boosting

```
while Number of constituents > 20 do
  while At least one constituent outside of  $\Delta R = 1$  from jet axis do
    Boost jet in  $z$  direction until  $\eta_{Jet} = 0$ 
    Rotate jet about  $z$  axis until  $\phi_{Jet} = 0$ 
    Rescale jet mass to 0.25 GeV
    Boost jet along its axis until  $E_{Jet} = 1$  GeV
    Rotate jet about  $x$  axis until hardest constituent has  $\eta_1 = 0, \phi_1 > 0$ 
    if Any constituents have  $\Delta R > 1$  then
      Remove all constituents with  $\Delta R > 1$ 
      Rebuild jet with remaining constituents
    else
      break
    end
  end
  if Number of constituents > 20 then
    Keep up-to the first 20 constituents, ordered in  $p_T$ 
    Rebuild jet with remaining constituents
  else
    break
  end
end
end
Reflect constituents about  $\phi$  axis such that the second hardest constituent has  $\eta_2 > 0$ 
```

To evaluate the efficacy of this procedure, the model is trained on a dataset with 10% signal contamination both before and after pre-processing, and the resulting correlation between Anomaly Score and jet mass is compared. Figure 4 shows the two-dimensional distribution of the mass of the highest p_T (leading) jet in each event vs. its Anomaly Score before and after boosting the input jets. The results depict a significantly smaller amount of correlation between the jet's mass and its Anomaly Score, as desired.

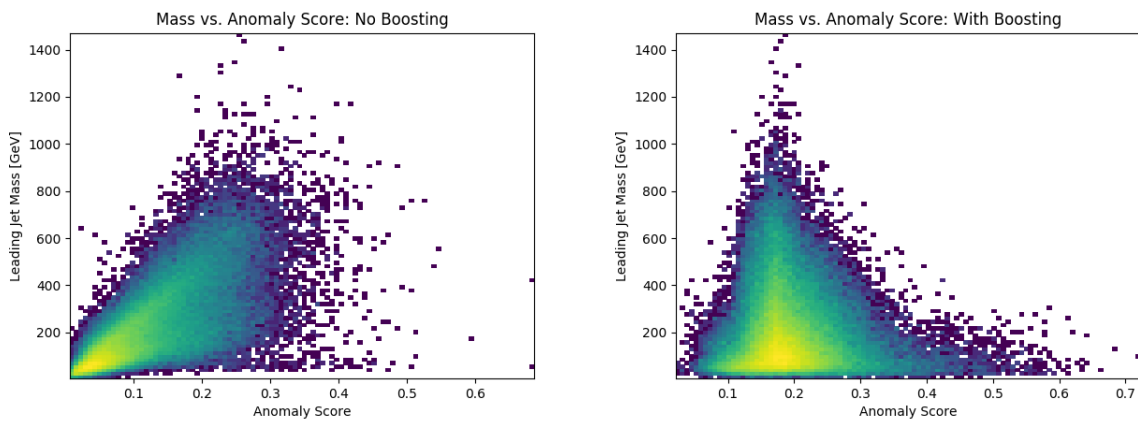


Figure 4: Leading Jet Mass vs Anomaly Score distributions before (left) and after (right) applying our boosting method

3.2 Sequence Ordering

In addition to this boosting method, the effect of *sequence ordering* on the input constituents has been investigated. In fixed architecture models, such as VAEs or image based Convolutional Neural Networks (CNNs), the ordering of constituents in the list of training inputs is seldom important. However, in recurrent architectures such as the VRNN, choosing a clever sequence ordering method that highlights important sequence features can boost performance.

The most intuitive method of ordering jet constituents is by their p_T in decreasing order, as harder constituents contribute more to a jet's substructure than softer constituents. The objective of this study is to build a model which can differentiate between diffuse jets resulting from soft QCD interactions, and jets with multiple cores resulting from the hadronic decay of boosted objects. Therefore, it is favorable to use a sequence ordering which makes the existence of multiple hard cores of a jet distinctly apparent. This is achieved by ordering the constituents in k_t -distance order. More specifically, the n^{th} constituent in the list is determined to be the constituent with the highest k_t -distance relative to the previous constituent, with the first constituent in the list being the highest p_T constituent.

$$c_n = \max(p_{Tn} \Delta R_{n,n-1}) \quad (16)$$

The effect on performance due to this choice of constituent ordering can be easily illustrated in the case of a two-prong jet. In such a case, the sequence will start with a constituent in one of the two cores of the jet, and be subsequently and consistently followed by a constituent belonging to the other core. This results in an easily predictable pattern which the VRNN is more able to model, particularly compared to a homogenous QCD jet. The resulting performance difference between p_T -sorted and k_t -sorted inputs is shown in Figure 5. Using the same 10% contaminated dataset, two-prong signal jets have a notably lower Anomaly Score when compared to background QCD jets due to the ease of modeling their substructure. (diagram maybe?)

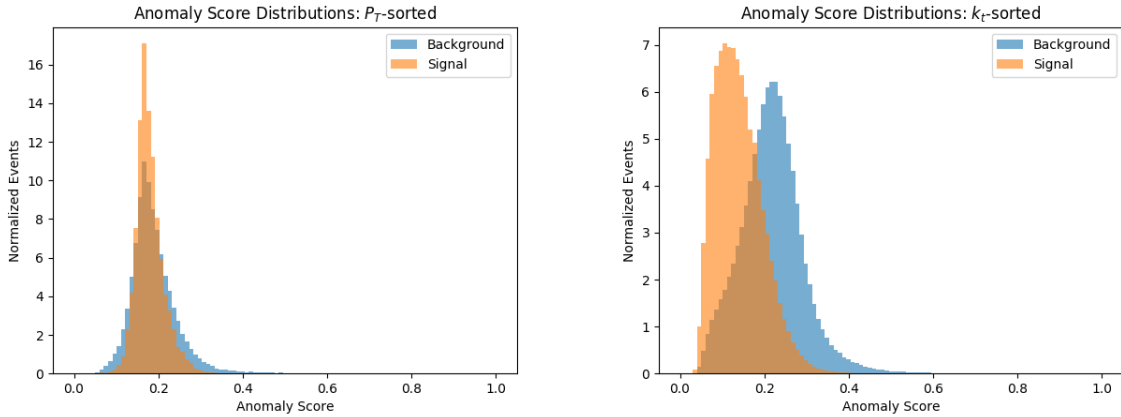


Figure 5: Leading jet Anomaly Score distributions for background and two-prong signal events, with p_T -sorted (left) and k_t -sorted (right) ordering of constituents for input jets.

287 4 Results

288 One way the VRNN's performance can be studied is by assessing signal acceptance and back-
289 ground rejection at the jet level by using only the leading jet of each event. In addition, the
290 Anomaly Score can be applied to both the X and Y jets in an event and used to discriminate
291 between signal and background in an event-level analysis context. Results of the VRNN's per-
292 formance are provided for both use cases in the following sections.

293 4.1 Jet Level Performance

294 In the jet-level assessment, the model is trained on the leading jets of each event for 500 epochs.
295 To evaluate the trend in performance during training, a computation of the Receiver Operating
296 Characteristic's Area Under the Curve (ROC AUC) is performed after each epoch by comparing
297 events in either the contaminated training set or the background-only validation set to those in
298 the signal-only set. Figure 6 shows the results of this training scenario in the case of 10%
299 contamination. Notably, the VRNN quickly reaches its optimal performance, and retains a
300 stable performance throughout the training period.

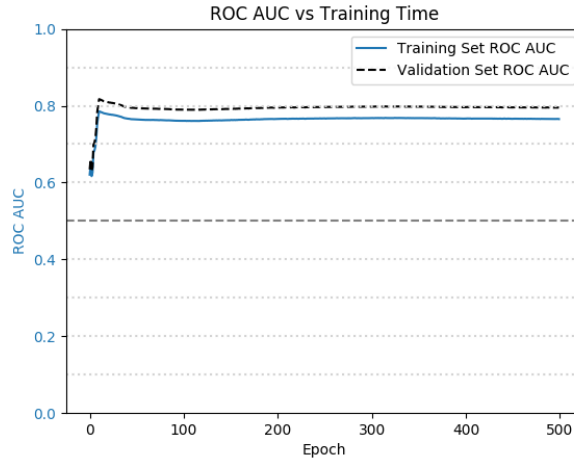


Figure 6: Area Under the Curve (ROC AUC) vs. training time in epochs. The VRNN reaches an optimal performance quickly, and retains this performance over a long training period. The difference in performance between the training and validation sets is a result of the former containing elements of signal.

301 Since the training scenario is entirely unsupervised, the resulting Anomaly Score distributions
302 from each training dataset may vary. To arrive at a consistent score distribution, a transformation
303 is applied on the resulting Anomaly Score which aims to satisfy two conditions:

- 304 • The mean of the resulting distribution is at an Anomaly Score value of 0.5.
- 305 • Anomaly scores closer to a value of 1 correspond to more signal-like jets.

306 The transformation per jet can be summarized as

$$\rho' = 1 - \left(\frac{\rho}{2\bar{\rho}} \right) \quad (17)$$

307 where ρ' is the transformed Anomaly Score, and $\bar{\rho}$ is the mean of the un-transformed Anomaly
308 Score distribution of the training set.

309 Figure 7 shows the mass distributions of the leading jet before and after a jet-level selection
310 requiring the Anomaly Score to exceed a value of 0.65. This value is chosen in the interest of
311 displaying the discriminating power of the Anomaly Score while maintaining a high enough
312 number of statistics to observe the variable's effect on the shape of the background. Notably,
313 the presence of the known resonances at 100 GeV and 500 GeV is enhanced. Sculpting in the
314 background distribution is observed, which is an effect of mass correlation mainly introduced
315 by the k_t -ordered sequencing, as there is a non-trivial correlation between the number of hard
316 cores in a jet and its mass. Both the signal enhancement and background sculpting are similarly
317 observed on three-pronged signatures in Figure 8, also shown in a 10% contaminated dataset.

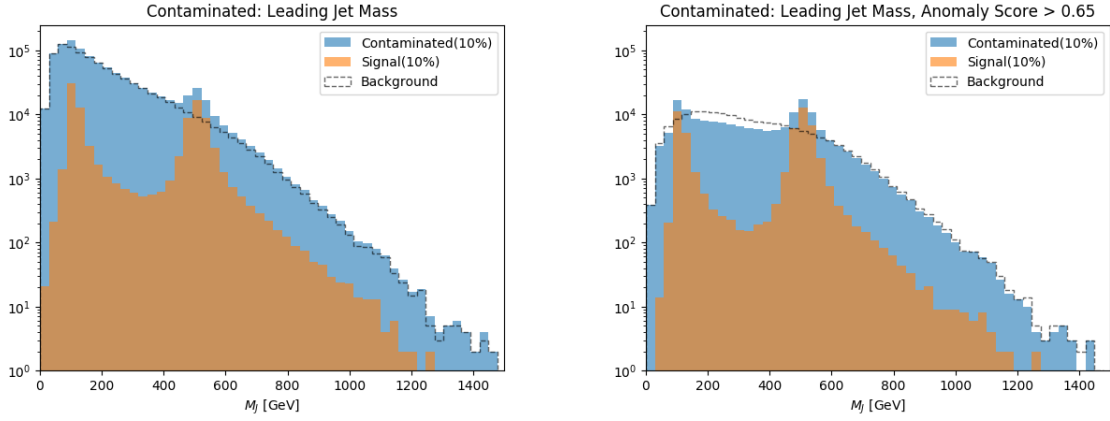


Figure 7: Leading jet mass distributions with a two-prong signal hypothesis before (left) and after (right) a cut on the Anomaly Score.

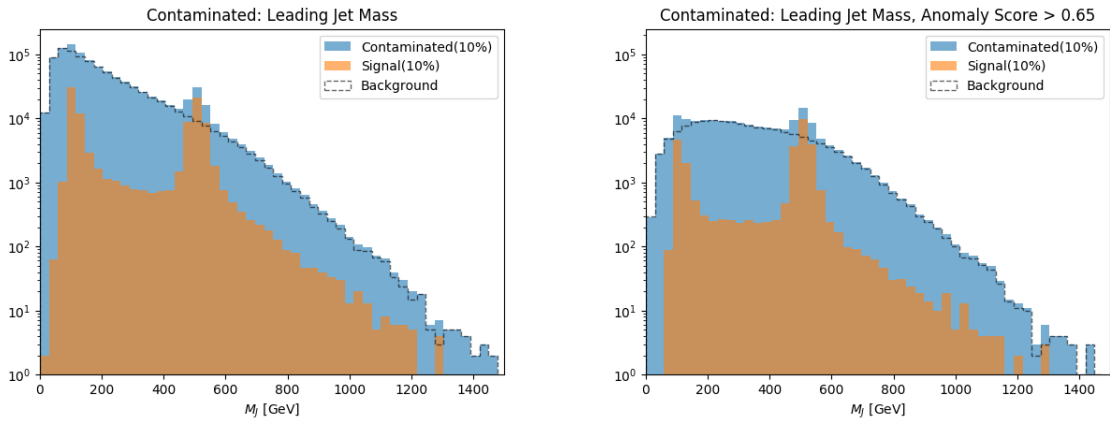


Figure 8: Leading jet mass distributions with a three-prong signal hypothesis before (left) and after (right) a cut on the Anomaly Score.

As the Anomaly Score in this context distinguishes two-pronged substructure from homogeneous jets, it is apt to compare to a commonly used high-level variable sensitive to two-pronged signals. The energy correlation function ratio D_2 [18] is selected and used as a benchmark to contextualize the Anomaly Score in both signal discrimination and jet mass correlation.

Figure 9 shows a comparison of the shapes of the contaminated jet mass distributions when subject to a cut on Anomaly Score and D_2 . The Anomaly Score is again selected to exceed a value of 0.65, and the D_2 selection is chosen to provide an equivalent background acceptance. The shape of the jet mass distribution is more significantly sculpted after the D_2 selection than the Anomaly Score selection, indicating more significant correlation of D_2 with jet mass while the Anomaly Score selection retains more of the smoothly falling characteristics of the background jet mass distribution. Such a result can be attributed largely to the boosting method used during pre-processing, as well as to the Anomaly Score being determined only from jet constituent four-vector information, without any high-level information being input into the model.

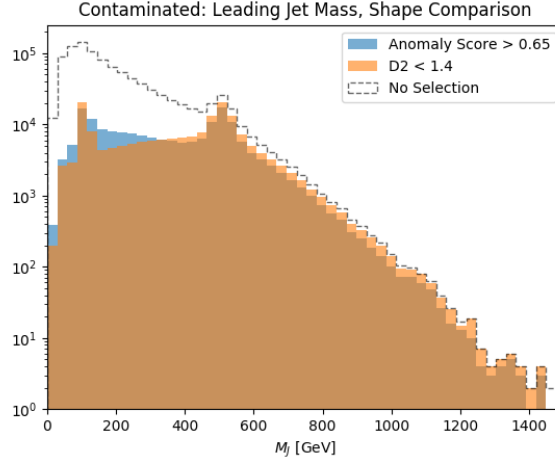


Figure 9: Contaminated set shape comparison between a selection on the Anomaly Score and a selection on the D_2 variable which provides an equivalent background acceptance. Notably, the D_2 variable causes more severe sculpting in the jet mass distribution than the Anomaly Score, indicating that selections on the Anomaly Score provide a more faithful representation of the original background mass distribution while still enhancing the presence of signal-like jets.

Another important study involves the model’s performance over a range of signal contamination levels. Figure 10 shows the ROC AUC values of both two and three-pronged signal hypotheses after training on each of the contaminated datasets as described in Section 3. At each level of contamination, the VRNN is trained on both the respective two-prong signal and three-prong signal contaminated datasets for 500 epochs. The resulting trained network is then used to assign an Anomaly Score to each jet in the dataset. AUC values for each level of contamination are determined from a ROC curve built from 1000 randomly selected jets from both the background and signal sets after training. Error bars are computed by repeating this process 100 times and determining the standard deviation of the resulting distribution of AUC values. Notably, the performance is consistent along all contaminations, and effective on both two and three-pronged signals without any prior substructure hypothesis. The Anomaly Score can therefore be interpreted as a quantity which is capable of adequately and consistently parametrizing multiple distinct substructure scenarios. This feature is valuable in model-independent searches,

344 or those without a pre-defined signal substructure hypothesis.

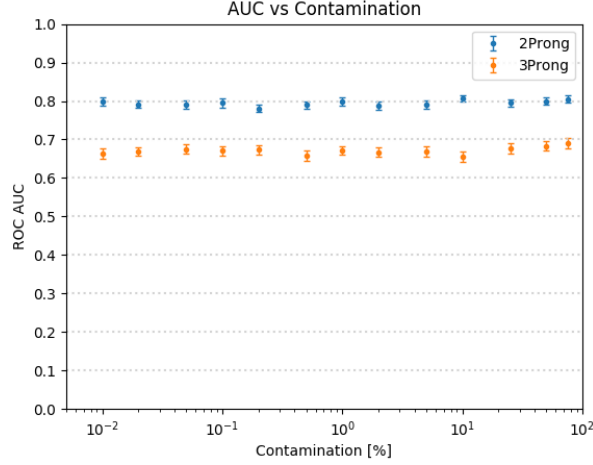


Figure 10: ROC AUC vs. signal contamination in training dataset, given as a percentage of the total events. The performance of the Anomaly Score is consistent across a wide range of contamination levels, indicating that the pre-processing method used is capable of providing a sequence of jet constituent four-vectors with salient substructure information. Data points for contamination levels up to and including 10% were determined from contaminated datasets all containing the same 895113 background events while varying the number of signal events. The three highest contamination amounts, corresponding to 25%, 50%, and 75%, were determined from contaminated datasets all containing the same 99547 signal events while varying the number of background events.

345 The ability of the Anomaly Score to be consistently performant along a large range of contam-
 346 inations is unexpected in the context of anomaly detection, where the dilution of the training
 347 set with a high number of signal elements is expected to result in lower performance. The
 348 consistent performance observed can be attributed to the choice of k_t -ordered sequencing and
 349 the representation of jets as variable-length sequences of constituents. Since the choice of k_t -
 350 ordered sequencing highlights the presence of multiple hard cores within a jet, the VRNN's
 351 Anomaly Score is predisposed to correlate with signal jets due to their anomalous substructure
 352 regardless of the level of contamination.

353 4.2 Event Level Performance

354 A natural benchmark of Anomaly Score's ability to distinguish anomalous jets is to apply the
 355 score in an analysis-like context. In this study, the goal is to reconstruct the Z' particle in the
 356 invariant mass spectrum M_{JJ} of the two jets in each signal event. To do this, the network is
 357 trained on both the leading and sub-leading jets of the event, with one set of network weights
 358 saved for each amount of contamination.

359 Since the model produces one Anomaly Score per jet, a combination of Anomaly Scores for the
 360 leading and sub-leading jet must be combined to arrive at an overall *Event Score*. In this study,
 361 the Event Score is chosen to be the highest of the two individual Anomaly Scores between the
 362 leading and sub-leading jets. This constructs an event-level discriminant which uses the most

anomalous jet in the event to discriminate. The ability of the Event Score to distinguish signal from background is illustrated in Figure 11, showing the correlations between the dijet invariant mass and the assigned Event Score in a dataset with 10% signal contamination. The significant feature of the 3500 GeV Z' occupies high values of the Event Score, validating the Event Score as a discriminant of anomalous events from background.

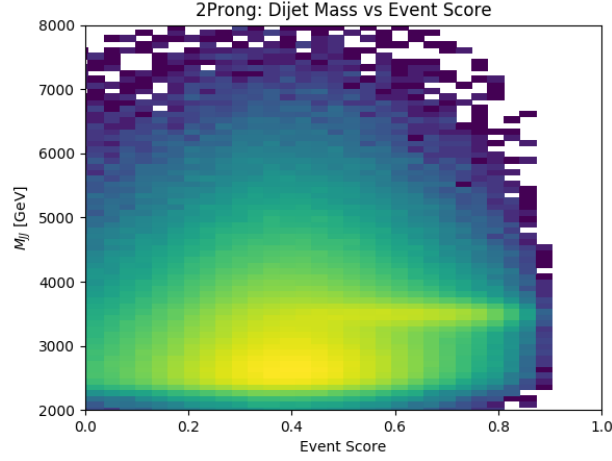


Figure 11: Dijet invariant mass vs. Event Score.

The goal of this search is to observe an excess of signal events in the dijet invariant mass distribution at a mass corresponding to the Z' particle. This is commonly referred to as a "bump hunt" search, in which the signal is expected to appear as a bump upon an otherwise smoothly falling background distribution.

Figure 12 shows the dijet mass distributions of the signal, background, and contaminated datasets, before and after applying a selection on the Event Score at a value of 0.65. This cut value was chosen such that the performance of the Anomaly Score is demonstrated while still retaining enough statistics to preserve the shape of the falling background distribution. Also plotted is the local significance σ in each bin of the corresponding histogram, where a total uncertainty of 15% on the number of background events is assumed. The local significance was computed using the BINOMALEXPZ function from ROOSTATS [19].

The requirement on the Event Score dramatically increases the significance of the excess from 0.5σ to 4σ at a signal contamination of 1.0%, while still retaining the smoothly falling behavior of the background. No selections other than the Event Score requirement have been applied in these scenarios besides the initial trigger requirement of $p_T > 1200 GeV$ on the leading jet. In Figure 13, a similar result is seen in the case of the three-pronged signal, where the Event Score requirement results in an increase of local significance of the signal peak from 0.5σ to 1.5σ at a signal contamination of 1% under the same conditions. These results display the capability of the Anomaly Score as an analysis variable, as it can distinguish signal events with multiple substructure hypotheses while being robust against ambiguities in signal jet mass and p_T .

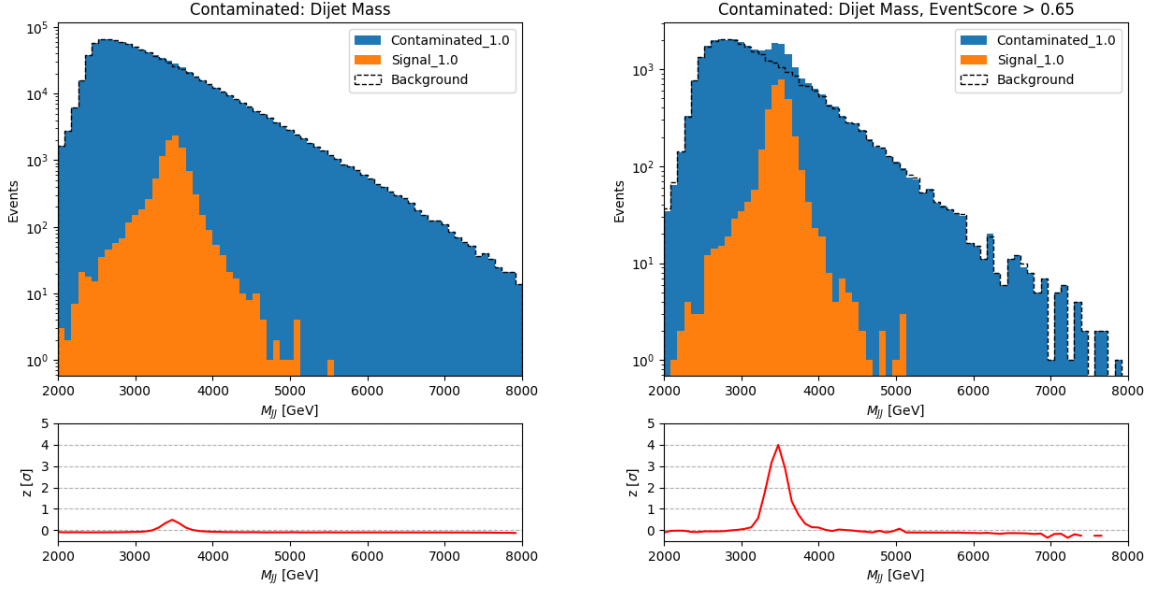


Figure 12: Two-prong dijet mass distributions before (left) and after (right) a cut on the Event Score, at a signal contamination of 1.0%. The Event Score selection provides a significant improvement in signal sensitivity from 0.5σ to 4σ while retaining the smoothly falling background distribution.

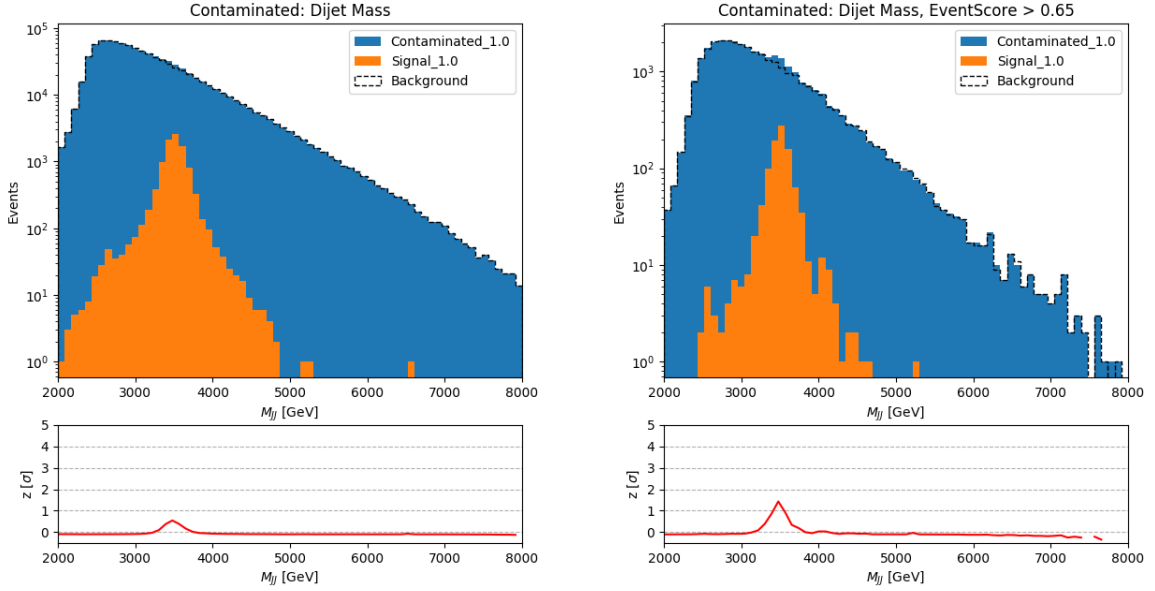


Figure 13: Three-prong dijet mass distributions before (left) and after (right) a cut on the Event Score, at a signal contamination of 1.0%. The Event Score selection provides an improvement in signal sensitivity from 0.5σ to 1.5σ while retaining the smoothly falling background distribution.

Conclusion

A novel approach for unsupervised signal identification in the context of new physics searches is presented. The technique utilizes a Variational Recurrent Neural Network trained on contaminated datasets to distinguish jets resulting from boosted hadronically decaying objects from those resulting from soft QCD processes. A precise pre-processing procedure is developed, in which each input jet is boosted to the same reference mass, energy, and orientation, coupled with a sequence ordering which makes the presence of signal-like substructure more apparent. The resulting training produces an Anomaly Score per jet that is sensitive to multiple substructure hypotheses. In a jet-level study that only uses leading jets in the dataset, the model enhances signal with less jet mass correlation than other traditional substructure variables such as D_2 . In addition, the resulting Anomaly Score is equally performant across varying levels of contamination, allowing for a consistent characterization of substructure regardless of the amount of signal present in the dataset. When applied to an event-level context, the Anomaly Score greatly increases the significance of signal excesses regardless of substructure hypothesis, while mostly retaining the smoothly falling shape of the background's mass distribution.

The Variational Recurrent Neural Network used in this study is a powerful tool capable of learning underlying features of physics objects presented as sequential data. Its applications to new physics searches are numerous, with one of the most attractive features being the potential for training directly on data without a pre-defined signal substructure hypothesis. It is also a general tool for modeling sequential data of any type, making it compatible with common high energy physics tasks such as supervised event-level searches or object-level classification.

The approach in this study is model-independent, in that it accommodates multiple substructure hypotheses. However, the model lends itself to a number of potential avenues for exploration into traditional supervised contexts as well, expanding its utility beyond the context of anomaly detection. Since the overall structure of the model contains both elements of Variational Autoencoders and Recurrent Neural Networks, more complicated architectural iterations can be employed as natural extensions of the VRNN. Examples of possible additions include adversarial mass de-correlation networks, and conditional architectures which can supplement the VRNN's input by a fixed length vector of high-level features. This study shows promising results for the application of the VRNN in unsupervised, model-independent object identification. However, exploration into additional avenues of study is warranted. Potential studies include further investigation of the ordering of the input constituent sequence, which may be tuned to accommodate better defined model hypotheses, or a study of multi-class identification in which two or more types of anomalies are identified within the same dataset.

Acknowledgements

The authors would like to thank Gregor Kasieczka, Ben Nachman, and David Shih, the organizers of the LHC Olympics 2020 Anomaly Detection Challenge, for providing the datasets used in this study and for the opportunity to develop and test the VRNN architecture.

This material is based upon work supported by the National Science Foundation under Grant No. PHY-2013070.

References and Notes

- [1] ATLAS Collaboration. Observation of a new particle in the search for the standard model higgs boson with the atlas detector at the lhc. *Physics Letters B*, 716(1):1–29, Sep 2012.
- [2] CMS Collaboration. Observation of a new boson at a mass of 125 gev with the cms experiment at the lhc. *Physics Letters B*, 716(1):30–61, Sep 2012.
- [3] Eric M. Metodiev, Benjamin Nachman, and Jesse Thaler. Classification without labels: learning from mixed samples in high energy physics. *Journal of High Energy Physics*, 2017(10), Oct 2017.
- [4] Dor Bank, Noam Koenigstein, and Raja Giryes. Autoencoders, 2020.
- [5] Marco Farina, Yuichiro Nakai, and David Shih. Searching for new physics with deep autoencoders. *Physical Review D*, 101(7), Apr 2020.
- [6] Theo Heimel, Gregor Kasieczka, Tilman Plehn, and Jennifer Thompson. Qcd or what? *SciPost Physics*, 6(3), Mar 2019.
- [7] Diederik P Kingma and Max Welling. Auto-encoding variational bayes, 2014.
- [8] Ian Goodfellow, Yoshua Bengio, and Aaron Courville. *Deep Learning*. MIT Press, 2016. <http://www.deeplearningbook.org>.
- [9] Jinwon An and S. Cho. Variational autoencoder based anomaly detection using reconstruction probability. 2015.
- [10] Junyoung Chung, Kyle Kastner, Laurent Dinh, Kratarth Goel, Aaron Courville, and Yoshua Bengio. A recurrent latent variable model for sequential data, 2016.
- [11] Sepp Hochreiter and Jürgen Schmidhuber. Long short-term memory. *Neural Comput.*, 9(8):1735–1780, November 1997.
- [12] Kyunghyun Cho, Bart van Merriënboer, Caglar Gulcehre, Dzmitry Bahdanau, Fethi Bougares, Holger Schwenk, and Yoshua Bengio. Learning phrase representations using rnn encoder-decoder for statistical machine translation, 2014.
- [13] Gregor Kasieczka, Ben Nachman, and David Shih. R&D Dataset for LHC Olympics 2020 Anomaly Detection Challenge, April 2019.
- [14] Matteo Cacciari, Gavin P Salam, and Gregory Soyez. The anti-kt jet clustering algorithm. *Journal of High Energy Physics*, 2008(04):063–063, Apr 2008.
- [15] Performance of mass-decorrelated jet substructure observables for hadronic two-body decay tagging in ATLAS. Technical Report ATL-PHYS-PUB-2018-014, CERN, Geneva, Jul 2018.
- [16] S. Purushotham, Wilka Carvalho, Tanachat Nilanon, and Y. Liu. Variational recurrent adversarial deep domain adaptation. In *ICLR*, 2017.
- [17] Tuhin S. Roy and Aravind H. Vijay. A robust anomaly finder based on autoencoders, 2020.

- 463 [18] Simone Marzani, Gregory Soyez, and Michael Spannowsky. Looking inside jets. *Lecture*
464 *Notes in Physics*, 2019.
- 465 [19] Lorenzo Moneta, Kevin Belasco, Kyle Cranmer, Sven Kreiss, Alfio Lazzaro, Danilo Pi-
466 paro, Gregory Schott, Wouter Verkerke, and Matthias Wolf. The roostats project, 2011.